Subterahertz Momentum Drag and Violation of Matthiessen's Rule in an Ultraclean Ferromagnetic $SrRuO_3$ Metallic Thin Film

Youcheng Wang,[1] G. Bossé,[1,2] H. P. Nair,[3] N. J. Schreiber,[3] J. P. Ruf,[4] B. Cheng,[1] C. Adamo,[3] D. E. Shai,[4] Y. Lubashevsky,[1] D. G. Schlom,[3,5] K. M. Shen,[4,5] and N. P. Armitage[1]

[1]*The Institute for Quantum Matter, Department of Physics and Astronomy, The Johns Hopkins University, Baltimore, Maryland 21218, USA*

[2]*Physics Department, University of North Florida, Jacksonville, Florida 32224-7699, USA*

[3]*Department of Materials Science and Engineering, Cornell University, Ithaca, New York 14853, USA*

[4]*Laboratory of Atomic and Solid State Physics, Department of Physics, Cornell University, Ithaca, New York 14853, USA*

[5]*Kavli Institute at Cornell for Nanoscale Science, Ithaca, New York 14853, USA*

(Received 23 March 2020; revised 14 August 2020; accepted 9 October 2020; published 16 November 2020)

$SrRuO_3$, a ferromagnet with an approximately 160 K Curie temperature, exhibits a T^2-dependent dc resistivity below ≈30 K. Nevertheless, previous optical studies in the infrared and terahertz range show non-Drude dynamics at low temperatures, which seem to contradict Fermi-liquid predictions. In this work, we measure the low-frequency THz range response of thin films with residual resistivity ratios, $\rho_{300K}/\rho_{4K} \approx 74$. At temperatures below 30 K, we find both a sharp zero frequency mode which has a width narrower than $k_BT/\hbar$ as well as a broader zero frequency Lorentzian that has at least an order of magnitude larger scattering. Both features have temperature dependences consistent with a Fermi liquid with the wider feature explicitly showing a T^2 scaling. Above 30 K, there is a crossover to a regime described by a single Drude peak that we believe arises from strong interband electron-electron scattering. Such two channel Drude transport sheds light on reports of the violation of Matthiessen's rule and extreme sensitivity to disorder in metallic ruthenates.

DOI: 10.1103/PhysRevLett.125.217401

The 4*d* ruthenates are well suited to the study of itinerant correlated electrons and the stability of the Fermi-liquid state because no explicit doping is necessary to produce metallic conduction [1–5]. The position of the Fermi level in bands resulting from the hybridization of O 2*p* and Ru 4*d* leads to ground-state behavior ranging from ferromagnetism in $SrRuO_3$, metallic paramagnetism in $CaRuO_3$ [6], insulating antiferromagnetism in Ca_2RuO_4, quantum critical metamagnetism in $Sr_3Ru_2O_7$ [7], and unconventional superconductivity in Sr_2RuO_4 [5]. These materials present an opportunity to investigate correlated electrons in the low-disorder limit.

$SrRuO_3$ exhibits a transition from a paramagnetic to a ferromagnetic state at $T_c \approx 160$ K. Quantum oscillations and a quadratic temperature dependence of the resistivity have been measured in the highest-quality samples [4,8]. These findings suggest that the ground state of $SrRuO_3$ is a magnetic Fermi liquid. Anomalous Hall and magneto-optical measurements suggest the existence of intrinsic Berry phase effects near the Fermi energy [9,10]. Nevertheless, among other experimental observations, infrared and optical measurements of $SrRuO_3$ films (that generally have had higher-disorder levels than single crystals) have shown a finite frequency peak in σ_1 at frequencies of order $3k_BT$ [11]. At frequencies above the peak, the real part of the optical conductivity was observed to fall off as $\omega^{-1/2}$ [11]. Optical measurements at lower frequency gave evidence for a related fractional power law dependence of the conductivity on the transport relaxation time [12]. The theoretical basis to understand this seeming deviation from the Lorentzian Drude form (and by implication the non-Fermi-liquid nature of this material) is not clear considering the radical implications it would have on the link between ac and dc electrical transport. Similar deviations from simple Drude forms of finite frequency peaks and anomalous power laws have been seen in the related compound $CaRuO_3$ [6,13]. In addition, $SrRuO_3$ has a very striking negative deviation from Matthiessen's rule when impurity scattering is increased through electron irradiation. It was demonstrated that although the fractional form works for more disordered samples, it does not account for this violation for low-disorder samples [14,15]. These results highlight the extreme sensitivity to disorder in this material and the apparent dependence of even the inelastic scattering on sample quality. Therefore, measuring low-disorder $SrRuO_3$ samples at low energies would provide a unique opportunity to examine Fermi-liquid predictions in this strongly correlated material. Previous studies were performed at higher frequencies and/or on samples with larger disorder. Recently, extremely low-disorder films were grown of which photoemission measurements reveal a complement of heavy low energy bands [16].

In this Letter, we use time domain terahertz spectroscopy (TDTS) to examine the complex conductivity and resistivity of very-high-quality thin films of $SrRuO_3$. Below 30 K, we find the real part of the THz conductivity exhibits two very distinct low energy peaks that are related to different conduction channels. There is both a very sharp zero frequency conducting mode which has a width narrower than $k_BT/\hbar$ as well as a broader Lorentzian peak with at least an order of magnitude larger scattering rate. Both features have temperature dependences consistent with a Fermi liquid with the wider feature explicitly showing a T^2 scaling. There are a number of possibilities for the origin of these features including multiband effects that arise from momentum conserving interband scattering and the approximate conservation of a pseudomomentum that arises from this material's quasi-1D Fermi surface sheets. Above 30 K, there is a crossover to a regime described by a single Drude peak that we believe arises from strong interband electron-electron scattering.

In TDTS, an approximately 1 ps long electromagnetic pulse is transmitted through a substrate and film. The complex transmission $T(\omega)$ is obtained from the Fourier transform of the time trace referenced to a bare substrate. Complex conductivity $\sigma(\omega)$ is calculated without the need for Kramers-Kronig transformation from the complex transmission using $T(\omega) = [(1+n)/1+n+\sigma(\omega)dZ_0]e^{[(i\omega\Delta L(n-1))/(c)]}$. In this expression, n is the substrate index, ΔL is a correction that accounts for thickness differences between the reference substrate and the sample substrate, d is the film thickness, and Z_0 is the impedance of free space (377 Ω). We determined the effective ΔL from a self-consistent first echo measurement of the sample and substrate at different temperatures. The proper determination of ΔL to submicron accuracy is essential for the accuracy of these results [17]. The films were grown on single-crystal $DyScO_3$ (110) substrates by molecular-beam epitaxy to a thickness of 23 nm [17]. Because this substrate is very lossy to the THz signal in the [001] direction (see Supplemental Material [17] Fig. S3), in all presented measurements the polarization of the incident THz beam is aligned parallel to the $[\bar{1}10]$ direction. Our data on samples grown on less lossy (and more highly strained) $NdGaO_3$ substrates show that the in-plane anisotropy is less than 20% with no qualitative difference between the two directions (Supplemental Material [17] Fig. S4).

dc resistivity $\rho(T)$ was measured in the van der Pauw geometry and anisotropy determined from the Montgomery method [28] [Fig. 1(a)]. The kink at 168 K is attributed to the development of ferromagnetic order [29]. The high quality of the film is reflected in its low residual resistivity of $\rho(T \to 0) \sim 2.6\ \mu\Omega\,\mathrm{cm}$ giving a large residual resistivity ratio of ≈74 along the $[\bar{1}10]$ direction. This residual resistivity is almost 20 times lower than the films used in previous TDTS studies [12]. A quadratic dependence on the temperature of $\rho(T) - \rho(0)$ has been reported up to at least 30 K [inset of Fig. 1(a)]. Our observation of a T^2 dependence of the resistivity is consistent with other studies on low-disorder samples [8,30] as opposed to behavior T^β, where $\beta \sim 1$–2 is observed primarily in samples with residual resistivities above 50 $\mu\Omega\,\mathrm{cm}$ [29].

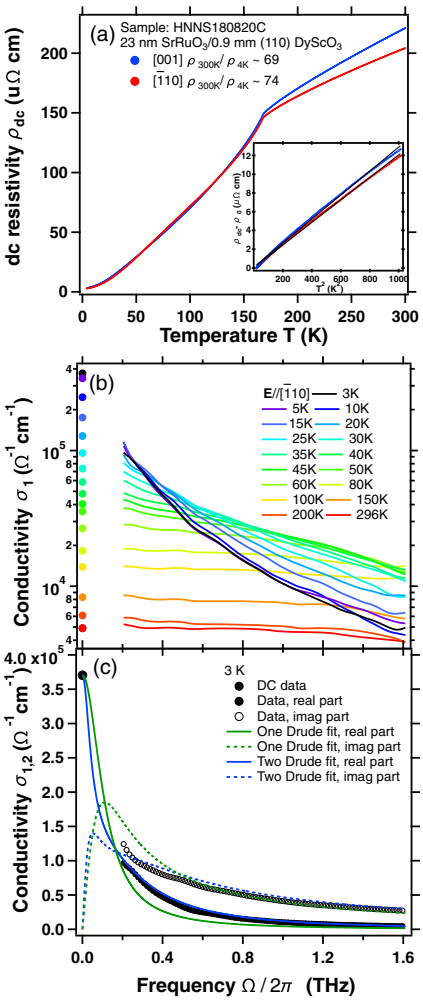

FIG. 1. (a) dc resistivity as a function of the temperature for the $SrRuO_3$ film for the two orthogonal directions. Inset: resistivity minus residual resistivity as a function of T^2. Fits to the data in the temperature range 2–32 K are shown as black lines. (b) Real part of the THz conductivity σ_1 from 5 K to room temperature along with corresponding dc values. (c) One Drude vs two Drude fit of dc and THz data at 3 K. The dc conductivity and real and imaginary parts of the complex conductivity are fitted simultaneously.

In Fig. 1(b), we plot the real part of the THz and dc conductivity at different temperatures. With decreasing temperature, there is a remarkable sharpening of a low-frequency Drude-like peak. The real σ_1 and imaginary σ_2 parts of the complex conductivity, with corresponding dc values at 3 K are plotted in Fig. 1(c). At this temperature, the peak in σ_1 is so narrow that $\sigma_2 > \sigma_1$ for the entire frequency range measured. In a simple single-band metal, one expects that the scattering of electrons is dominated by quenched disorder as $T \to 0$ and that the dynamical

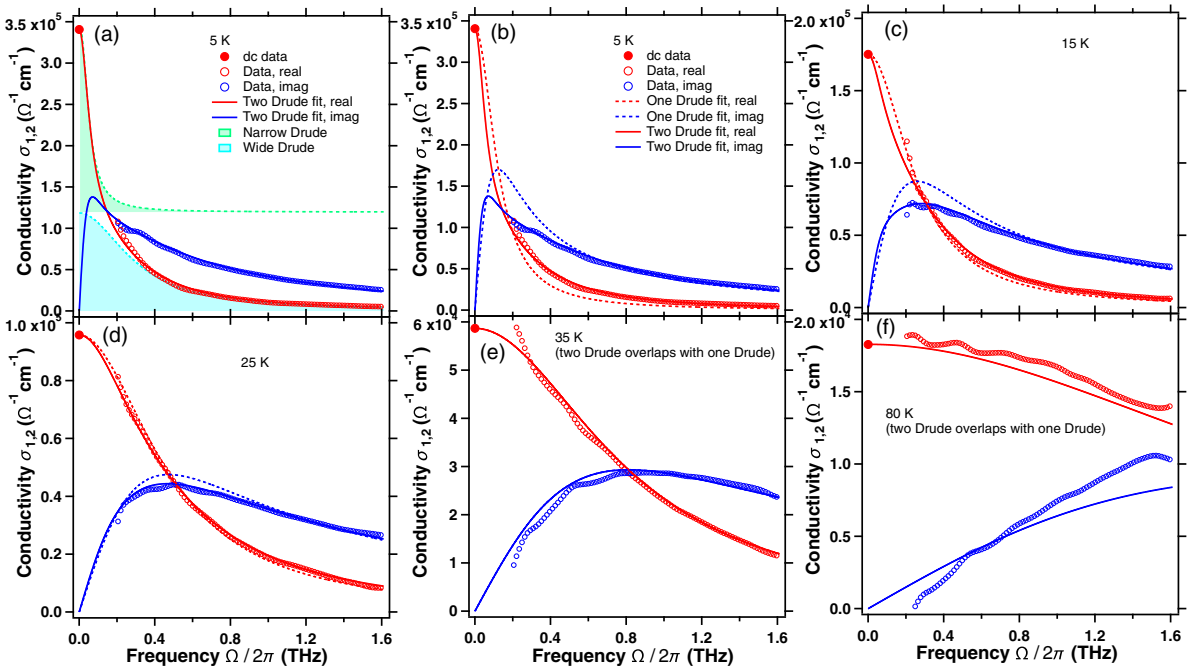

FIG. 2. (a) Real and imaginary THz conductivity with dc values at 5 K. The red and blue solid lines show fitting with two Drude terms. The green and blue shaded regions correspond to a narrow and wider Drude term, respectively. The green shade is offset to distinguish from the other. (b)–(f) Real and imaginary parts of the complex conductivity with dc values for 5 K [same data as in (a)], 15, 25, 35, and 80 K. The data are presented with one Drude (dashed lines) and two Drude modeling (solid lines). Note that for 35 and 80 K, two Drude terms from fitting have the same scattering rates, so the two Drude overlaps with one Drude fitting. In (b)–(f) the same line types are used.

conductivity can be modeled with a single Drude oscillator with the functional form $\sigma(\omega) = \epsilon_0[(\omega_p^2)/(1/\tau - i\omega)]$ (where ω_p is the plasma frequency and $1/\tau$ is the current decay rate). Although the σ_1 data superficially have such a Drude form, the 3 K complex conductivity, in fact, cannot be reproduced with a single Drude oscillator. As can be seen in Fig. 1(c), the best fits with a single Drude oscillator to the THz constrained with the dc resistivity underestimates the real conductivity and overestimates the imaginary conductivity. Note that we can make such an assessment despite the fact that the spectral range between dc and 200 GHz is not measured because the real and imaginary parts of σ are Kramers-Kronig related to each other; e.g., the data are strongly constrained for parts of the spectral range that are not explicitly measured, by parts that are measured. In order to fit the 3 K conductivity, at least two Lorentzian oscillators are needed: one narrow with $1/\tau_1 \lesssim 50$ GHz scattering rate and one wider with $1/\tau_2 \sim$ 300 GHz scattering rate. Because the narrow oscillator has a width below the measured frequency range, we can only set an upper limit on its width, although we are highly sensitive to its spectral weight. In these fits, we adopt the highest value of $1/\tau_1$ consistent with THz data as its upper bound. The full functional form is $\sigma(\omega) = \sum_{n=1}^{2} \epsilon_0 {\omega_{p_n}}^2 [1/(1/\tau_n - i\omega)] - i\epsilon_0(\epsilon_\infty - 1)\omega$. ϵ_∞ accounts for effects of interband transitions at frequencies well above our range. As discussed below, the appearance of multiple Lorentzian Drude peaks is a natural expectation for a multiband metal.

The necessity to use two Drude terms extends to higher temperatures. One can see in the 5 K conductivity [Fig. 2(a)] that the narrow Drude (green area under the real part of the narrow Drude) accounts for the sharp upturn toward the dc conductivity, whereas the wide Drude part (blue) is needed to capture the long tail of $\sigma_1(\omega)$. In the data up to 30 K [Figs. 2(b) and 2(c)], one cannot fit the imaginary part of the conductivity with a single Drude if one insists on a fit of the real part. As the temperature increases, the scattering rate of the narrow Lorentzian increases faster than the scattering rate of the wider one, and the rates become equal above 30 K and the Lorentzians indistinguishable. Hence, a single Drude fitting above 30 K suffices. It is interesting to note that this temperature is close to that below which T^2 resistivity has been reported. The scattering rate of the wide Drude peak goes as T^2 below 30 K. The total spectral weight [Fig. 3(b)] is unchanged within 5% below 30 K, while the narrow Drude peak corresponds to about 20% of the total weight in the range where it can be distinguished. Note that the fractional functional form used previously [12] does not fit our data (Supplemental Material [17] Sec. IV). Also note that we see no sign of meV range finite frequency peaks arising from either finite temperature effects as observed previously in higher-disorder samples [11] or

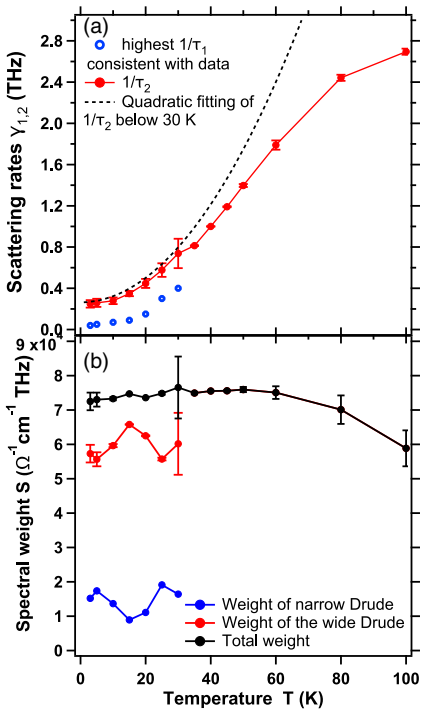

FIG. 3. (a) Scattering rate of the wide (red) and narrow (blue) Drude peaks as a function of T. The dashed line is a quadratic fit to the data below 30 K, and extended to higher T. (b) Spectral weight of the two Drude peaks (obtained from two Drude fitting) and their total spectral weight, from 5 to 30 K. Above 30 K, single Drude fit parameters are given. The spectral weight is proportional to ω_p^2.

that have been predicted to arise from the tilt of the octahedra [31].

We examined complex resistivity which is the inverse of complex conductivity data [17]. For a single-band metal, the "Gurzhi" scaling [32] for a metal with dominant umklapp scattering as $T \to 0$ predicts the real part of the resistivity goes as $\rho_1(T,\omega) = \rho_0^{ee}(T)[1 + (\hbar\omega)^2/b\pi^2(k_BT)^2]$ where $\rho_0^{ee}(T)$ is the quadratic dc resistivity. This relation arises from the established relation between T- and ω-induced inelastic scattering [33]. With the b that is predicted to be 4 for a canonical Fermi liquid, the scattering is dominated in our temperature and frequency range by the temperature; e.g., the broadening at 30 K at zero frequency is expected to be approximately 16.6 times larger than the broadening at 1 THz at $T = 0$. This is consistent with our data in that we find very little frequency-dependent changes to ρ_1 (Supplemental Material [17] Figs. S6 and S7), while the T-dependence changes are large. When intraband scattering processes dominate, the complex resistivity can be related to the "extended" Drude model (EDM), in which the scattering rate and effective masses in the Drude formula become complex and frequency dependent [34]. The EDM has been used extensively to describe heavy fermion systems [35,36], high-T_c cuprates [2], and transition-metal compounds [37]. Within the context of EDM, the slope of the imaginary part of the complex resistivity with frequency is proportional to the optical renormalized mass (m^*/m_b; m_b is the effective band mass). It is found that in our TDTS data, mass enhancement at the lowest temperatures is ~6.5 [Supplemental Material [17] Fig. S6(b)], which roughly agrees with heat capacity and de Haas–van Alphen measurements [29,38]. In particular, heat capacity measurements show a Sommerfeld coefficient $\gamma_{\text{expt}}/\gamma_{\text{theor}} = 3.7$, suggesting a mass enhancement similar to what we observe in TDTS measurements [29]. According to an angle-resolved de Haas–van Alphen study, the effective mass of charge carriers measured for each Fermi surface sheet ranges from 4.1 to $6.9m_e$ [38]. Similarly, angle-resolved photoemission has found masses of order $3.7m_e$ [16] for the β sheet.

We now discuss the possible origins of the multiple low-frequency Drude peaks and the crossover to a single peak at higher temperature. As mentioned above, one expects in a multiband metal like $SrRuO_3$ a number of independent conduction channels. In the low-temperature limit, disorder scattering is expected to be dominant, and the different channels will manifest as different Lorentzian Drude peaks. These may have very different residual widths as the rate of scattering by short-range impurities is proportional to the density of states of the band, which may be very different between bands. At high temperatures, electron-electron scattering will dominate. In an almost compensated metal such as $SrRuO_3$, scattering serves to equalize net velocities between electrons and hole bands giving rise to a single Drude peak [33,39]. This crossover scenario is quite general and discussed in more detail in the Ref. [17]. In a different scenario, Rosch and Andrei have shown [40,41] that in 1D it is possible to define a pseudomomentum that does not decay by two-particle collisions and hence decays more slowly than the conventional crystal momentum. It is expected that a state with finite pseudomomentum has significant projection on current-carrying states. This gives rise to well-defined and sharp peaks in the optical conductivity. One might expect these effects in even quasi-2D metals like $SrRuO_3$ as its Fermi surface is composed of primarily 1D sections that show only weak hybridization where the bands intersect. Irrespective of the mechanism, what these scenarios share is the idea that scattering channels *add* in the conductivity not the resistivity. The latter is the usual Matthiessen rule, and in this regard, our results give understanding of the deviations from Matthiessen's rule in this material.

We have examined THz dynamical conductivity in clean films of $SrRuO_3$, which have more than an order of magnitude smaller residual resistivity than previously measured samples, and observed very different results. At low temperature, a narrow Drude-like peak emerges, which cannot be parametrized with a single oscillator. As it is the low-frequency and low-temperature properties of a

system which are diagnostic of its ground state, the T^2 dependence of the widths of the low energy conductivity peaks confirm the Fermi-liquid nature of this compound. The presence of multiple Drude peaks, however, indicates effects beyond conventional Boltzmann transport and might help explain previous reports of deviations from Matthiessen's rule. They may indicate either the presence of extremely strong momentum-conserving electron-electron interactions or an almost conserved pseudomomentum due to quasi-1D Fermi surfaces of this system.

We would like to thank S. Dodge, S. Gopalakrishnan, D. Maslov, and J. Orenstein for helpful conversations. Work at J. H. U. was supported though the National Science Foundation (NSF) Grant No. DMR-1905519. Research at Cornell was supported by the NSF (Platform for the Accelerated Realization, Analysis and Discovery of Interface Materials) under Grant No. DMR-1539918. N. J. S. acknowledges support from the NSF Graduate Research Fellowships Program (GRFP) under Grant No. DGE-1650441. Work by D. E. S., J. P. R., and K. M. S. was supported by the NSF through Grant No. DMR-1709255. This research is funded in part by the Gordon and Betty Moore Foundations (GBMF) Emergent Phenomena in Quantum Systems (EPiQS) Initiative through Grant No. GBMF3850 to Cornell University. This work made use of the CCMR Shared Facilities, which are supported through the NSF MRSEC Program (Grant No. DMR-1719875). Substrate preparation was performed in part at the Cornell NanoScale Facility, a member of the National Nanotechnology Coordinated Infrastructure, which is supported by the NSF (Grant No. ECCS-1542081). Y. Wang would like to thank Ludi Miao for argon milling of a thin strip sample for microwave measurements [17].

[1] G. Koster, L. Klein, W. Siemons, G. Rijnders, J. S. Dodge, C.-B. Eom, D. H. A. Blank, and M. R. Beasley, Rev. Mod. Phys. **84**, 253 (2012).
[2] A. V. Puchkov, D. N. Basov, and T. Timusk, J. Phys. Condens. Matter **8**, 10049 (1996).
[3] Y. Maeno, Physica (Amsterdam) **282C–287C**, 206 (1997).
[4] L. Capogna, A. P. Mackenzie, R. S. Perry, S. A. Grigera, L. M. Galvin, P. Raychaudhuri, A. J. Schofield, C. S. Alexander, G. Cao, S. R. Julian *et al.*, Phys. Rev. Lett. **88**, 076602 (2002).
[5] R. S. Perry, L. M. Galvin, S. A. Grigera, L. Capogna, A. J. Schofield, A. P. Mackenzie, M. Chiao, S. R. Julian, S. Ikeda, S. Nakatsuji, Y. Maeno, and C. Pfleiderer, Phys. Rev. Lett. **86**, 2661 (2001).
[6] S. Kamal, D. M. Kim, C. B. Eom, and J. S. Dodge, Phys. Rev. B **74**, 165115 (2006).
[7] S. Grigera, R. Perry, A. Schofield, M. Chiao, S. Julian, G. Lonzarich, S. Ikeda, Y. Maeno, A. Millis, and A. Mackenzie, Science **294**, 329 (2001).
[8] A. P. Mackenzie, J. W. Reiner, A. W. Tyler, L. M. Galvin, S. R. Julian, M. R. Beasley, T. H. Geballe, and A. Kapitulnik, Phys. Rev. B **58**, R13318 (1998).
[9] Z. Fang, N. Nagaosa, K. S. Takahashi, A. Asamitsu, R. Mathieu, T. Ogasawara, H. Yamada, M. Kawasaki, Y. Tokura, and K. Terakura, Science **302**, 92 (2003).
[10] N. Hosaka, H. Yamada, Y. Shimada, J. Fujioka, S. Bordács, I. Kézsmárki, M. Kawasaki, and Y. Tokura, Appl. Phys. Express **1**, 113001 (2008).
[11] P. Kostic, Y. Okada, N. C. Collins, Z. Schlesinger, J. W. Reiner, L. Klein, A. Kapitulnik, T. H. Geballe, and M. R. Beasley, Phys. Rev. Lett. **81**, 2498 (1998).
[12] J. S. Dodge, C. P. Weber, J. Corson, J. Orenstein, Z. Schlesinger, J. W. Reiner, and M. R. Beasley, Phys. Rev. Lett. **85**, 4932 (2000).
[13] Y. S. Lee, J. Yu, J. S. Lee, T. W. Noh, T.-H. Gimm, H.-Y. Choi, and C. B. Eom, Phys. Rev. B **66**, 041104(R) (2002).
[14] L. Klein, Y. Kats, N. Wiser, M. Konczykowski, J. Reiner, T. Geballe, M. Beasley, and A. Kapitulnik, Europhys. Lett. **55**, 532 (2001).
[15] Y. Kats and L. Klein, Physica (Amsterdam) **312B–313B**, 793 (2002).
[16] D. E. Shai, C. Adamo, D. W. Shen, C. M. Brooks, J. W. Harter, E. J. Monkman, B. Burganov, D. G. Schlom, and K. M. Shen, Phys. Rev. Lett. **110**, 087004 (2013).
[17] See Supplemental Material at http://link.aps.org/supplemental/10.1103/PhysRevLett.125.217401 Sec. II for details about the measurement of δ_L, which includes Ref. [18], for the extended Drude analysis, which includes Refs. [19,20], and for the attempts to measure the microwave conductivity, which includes Refs. [21,22]. Section I for details about sample growth, which includes Refs. [23–25]. Section VII for the modeling of the conductivity of a two-band metal, which includes Refs. [26,27].
[18] A. B. Sushkov, G. S. Jenkins, D. C. Schmadel, N. P. Butch, J. Paglione, and H. D. Drew, Phys. Rev. B **82**, 125110 (2010).
[19] I. I. Mazin and D. J. Singh, Phys. Rev. B **56**, 2556 (1997).
[20] I. I. Mazin and D. J. Singh, Phys. Rev. B **73**, 189903(E) (2006).
[21] W. Liu, Ph.D. Thesis, The Johns Hopkins University, 2013.
[22] M. Scheffler, S. Kilic, and M. Dressel, Rev. Sci. Instrum. **78**, 086106 (2007).
[23] H. P. Nair, Y. Liu, J. P. Ruf, N. J. Schreiber, S.-L. Shang, D. J. Baek, B. H. Goodge, L. F. Kourkoutis, Z.-K. Liu, K. M. Shen *et al.*, APL Mater. **6**, 046101 (2018).
[24] D. B. Kacedon, R. A. Rao, and C. B. Eom, Appl. Phys. Lett. **71**, 1724 (1997).
[25] F. Chu, Q. Jia, G. Landrum, X. Wu, M. Hawley, and T. Mitchell, J. Electron. Mater. **25**, 1754 (1996).
[26] P. F. Maldague and C. A. Kukkonen, Phys. Rev. B **19**, 6172 (1979).
[27] W. G. Baber, Proc. R. Soc. A **158**, 383 (1937).
[28] H. Montgomery, J. Appl. Phys. **42**, 2971 (1971).
[29] P. B. Allen, H. Berger, O. Chauvet, L. Forro, T. Jarlborg, A. Junod, B. Revaz, and G. Santi, Phys. Rev. B **53**, 4393 (1996).
[30] G. Cao, O. Korneta, S. Chikara, L. DeLong, and P. Schlottmann, Solid State Commun. **148**, 305 (2008).
[31] H. T. Dang, J. Mravlje, A. Georges, and A. J. Millis, Phys. Rev. Lett. **115**, 107003 (2015).

[32] R. N. Gurzhi, Sov. Phys. JETP **8**, 673 (1959), http://www.jetp.ac.ru/cgi-bin/dn/e_008_04_0673.pdf.
[33] D. L. Maslov and A. V. Chubukov, Rep. Prog. Phys. **80**, 026503 (2017).
[34] D. N. Basov and T. Timusk, Rev. Mod. Phys. **77**, 721 (2005).
[35] B. C. Webb, A. J. Sievers, and T. Mihalisin, Phys. Rev. Lett. **57**, 1951 (1986).
[36] L. Degiorgi, Rev. Mod. Phys. **71**, 687 (1999).
[37] J. W. Allen and J. C. Mikkelsen, Phys. Rev. B **15**, 2952 (1977).
[38] C. S. Alexander, S. McCall, P. Schlottmann, J. E. Crow, and G. Cao, Phys. Rev. B **72**, 024415 (2005).
[39] V. Gantmakher and Y. Levinson, *Modern Problems in Condensed Matter Sciences Vol. 19: Carrier Scattering in Metals and Semiconductors* (Elsevier–North-Holland, New York 1987).
[40] A. Rosch and N. Andrei, J. Low Temp. Phys. **126**, 1195 (2002).
[41] A. Rosch, Ann. Phys. (Amsterdam) **15**, 526 (2006).